Transport properties of electromagnetic waves in dielectric photonic quasicrystals

Ekaterina E. Maslova [1,*] Vladislav A. Chistyakov [1] and Mikhail V. Rybin [1,2]
[1]*School of Physics and Engineering, ITMO University, 197101, St. Petersburg, Russia*
[2]*Ioffe Institute, 194021, St. Petersburg, Russia*

(Received 26 March 2024; revised 17 June 2024; accepted 24 June 2024; published 10 July 2024)

The transport properties of electromagnetic waves change at the transition of high-index dielectric photonic structures to the metamaterial regime. Here, we demonstrate the changes in the properties of the waves traveling through photonic quasicrystalline structures made of dielectric rods arranged in the nodes on a Penrose tiling lattice with C_5 rotation symmetry. We cannot use Bloch theorem in the study of aperiodic structures, so we consider full-scale structures to reveal Bragg- and Mie-type band gaps. A real-space metric allows us to define the period of the effective crystallographic planes in the quasicrystal and to relate the Bragg band gap to the lattice nodes in reciprocal space. We compared the quasicrystal structure with photonic crystals and found that transmission spectra in the band gap have similar profiles for both types of structures. The analysis of the magnetic field distribution in quasicrystal structures with high dielectric permittivity allowed us to recognize μ near-zero modes, which indicates that the structure acquires the metamaterial regime. The constructed phase diagram specified the metamaterial regime for the structure. Our results reveal the transport properties of photonic quasicrystalline systems in the metamaterial regime.

DOI: 10.1103/PhysRevB.110.014202

I. INTRODUCTION

Study of aperiodic systems in photonics has attracted considerable attention since they have richer physics than their counterparts with translation symmetry. Although the latter property enormously simplifies the analysis by using Bloch theorem providing solutions in the form of a plane wave and periodic function product, the wave vector restricts the waves to be either propagating (pure real wave vector) or evanescent waves (complex wave vector), which are localized at the sample boundary or other crystal imperfectness [1,2]. Among others, there are moire structures [3–5], hyperuniform structures [6,7], photonic glasses [8–11], Fourier surfaces [12–14], quasicrystals [15–18], and other quasicrystalline structures [19].

Aperiodic structures were reported to support effects that have already been observed in crystals and this uncovers that the translation symmetry is not necessary for them to appear. Observation of a clear diffraction pattern from quasicrystals was the first evidence of such structures to exist with a special type of atom arrangement in solids [20] and was recently reported for photonic structures [15,21–24]. A crystalline approximant, i.e., supercells containing quasicrystal fragments, shows a conical dispersion feature with the Dirac frequency, which is almost similar to those in structures with a hexagonal lattice [25]. Local density of photonic states was found to be suppressed and enhanced in ordered low-index quasicrystalline structures similar to those of periodic systems [19]. In addition, there are effects which are unique to aperiodic systems. In particular, quasicrystalline structures allow the opening of a complete photonic band gap in low-index samples made of polymer material [26,27]. Another example is an intrinsic wave localization in three-dimensional (3D) icosahedron quasicrystals [15,28], which is prohibited by Bloch theorem. The quasicrystalline approach also allows one to design structures that are almost transparent but only for incident waves with the desired frequency and angle of incidence [29,30].

High-index photonic structures with translation symmetry are known to acquire metamaterial properties [31] with near-zero index regimes [32]. The metamaterial regime appears when the local resonance supported by the constitutive elements becomes the fundamental resonance, i.e., its frequency is lower than that of any Bragg resonance. This transition to the metamaterial regime changes the transport properties of waves traveling through the structures. In particular, atom-based quasicrystals demonstrate different percolation regimes [33]. However, the study of transport properties of the photonic quasicrystalline systems has yet been carried out to date.

Here we report a study of the properties for a wave traveling through quasicrystal photonic structures made of dielectric rods arranged in nodes of lattice based on a Penrose tiling with C_5 rotation symmetry. Since Bloch theorem is inapplicable, we consider full-scale simulations to reveal Bragg- and Mie-type band gaps. To assign Bragg scattering to effective crystallographic planes, we developed a real-space metric, which also allows one to select several peaks in the reciprocal space, which are responsible to the Bragg band gap. We used a photonic crystal as a reference, which shows that quasicrystal structures have similar transmission suppression dependences on thickness in the band gap of both types. We recognize μ near-zero modes, which indicate that the structure

*Contact author: ekaterina.maslova@metalab.ifmo.ru

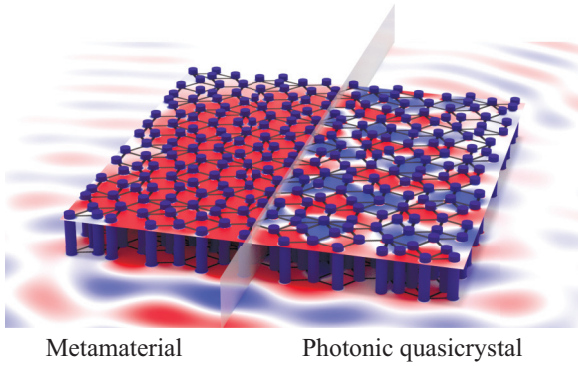

FIG. 1. Typical distribution of electromagnetic field in quasicrystal structure with Penrose-type lattice. On the left, the metamaterial regime with μ-near-zero regime and, on the right, typical distribution for photonic quasicrystal.

acquires a metamaterial regime (see Fig. 1). It allowed us to construct a phase diagram of the metamaterial regime in a structure with a quasicrystal lattice.

II. QUASICRYSTAL STRUCTURES

Several types of quasicrystalline structures are considered among many 2D aperiodic structures. Hyperuniform structures are designed with specified disorder to control the properties of electromagnetic waves [34,35]. Quasicrystalline structures in particular generated by merging an arbitrary number of lattices in the reciprocal space allows such structures to exhibit unique properties [12,30,36]. Quasicrystals are tiling based and resemble crystals more than the above mentioned ones. In most cases several unit cells form their aperiodic structures; however, recently a quasicrystal composed of a single unit cell was reported [37,38]. Penrose tiling [39] is a well-known example of aperiodic tilings, which was developed by Penrose even before the appearance of quasicrystals as a field in physics.

The Penrose tiling has a long-range order and C_5 rotation axis inconsistent with a translation symmetry. A convenient way to obtain a quasicrystal structure is the cut-and-projection method [40]. The Penrose tiling was constructed by projecting a five-dimensional hypercubic lattice onto a two-dimensional physical space and a three-dimensional space of projections [41]. In this case, the projection window is an icosahedron. When a shift parameter of the window $s = 0$, the icosahedron cross section of the xy planes appears as a pentagon. If a point of hypercube is inside the pentagons, the point is assigned to physical space and all of them form a tiling. The Penrose tiling comprises two types of rhombs: thin and thick ones. This indicates that the quasicrystal based on the Penrose tiling has two types of unit cells [Fig. 2(a)], in contrast to the regular crystals having only one type. The thick rhombi [shown in blue in Fig. 2(a)] have the angles of 108° and 72°, the larger diagonal d_1 equals $1.618a$ (the golden ratio), and the smaller $d_2 = 1.176a$, where a is constant lattice. The thin rhombi [red in Fig. 2(a)] have angles of 144° and 36°, the larger diagonal d_1 equals $1.902a$, and the smaller $d_2 = 0.618a$. The Penrose tiling has many configurations depending on the shift parameter s defining the offset of the projection window along

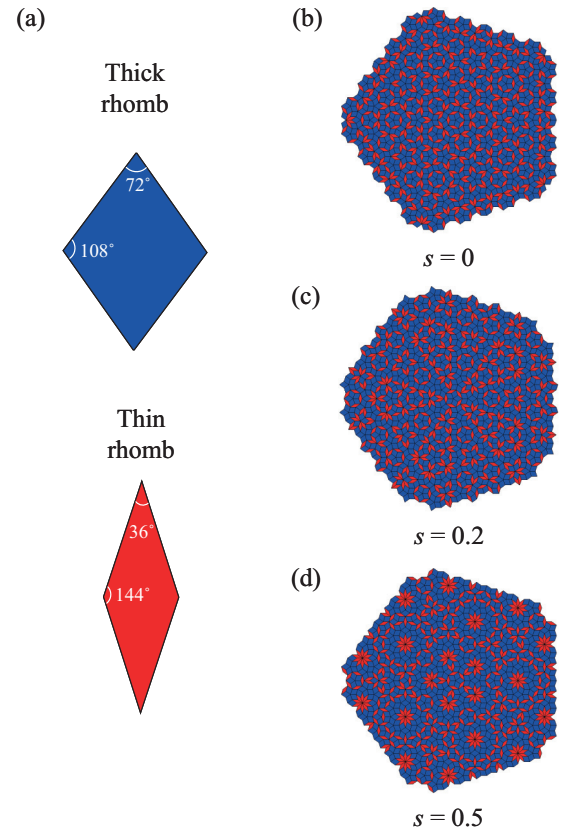

FIG. 2. Designs of the Penrose tilings constructed by using the cut-and-projection method with different shift parameters (a) $s = 0$, (b) $s = 0.2$, and (c) $s = 0.5$. Blue colors are for the thick rhombi; red colors are for the thin rhombi.

the z axis when one constructs a tiling using the projection method [41]. Here we consider three values of the shift parameter s: $s = 0$, $s = 0.2$, and $s = 0.5$, which provides us with a vast variability of the structures keeping their number quite reasonable.

III. STRUCTURAL FACTOR

We consider a quasicrystal lattice of dielectric rods of a radius r and a permittivity ε. Rods are arranged at the vertex of rhombi forming a Penrose tiling. A dependence of a lattice symmetry index (three for hexagonal, four for square, six for graphene lattices, and so on) and maximum filling fraction of rods with circular properties is known to be almost linear [42]. An extended Penrose lattice fits this linear dependence at symmetry index of five. The extended Penrose lattice has additional nodes at the centers of thick rhombi. Thus, in addition to the lattice, the nodes of which are at the rhomb vertices of a Penrose tiling, we considered the extended Penrose lattice.

In periodic structures, the metamaterial regime was determined by a change in the band diagram [43]. Periodic structures acquire metamaterial properties when the fundamental band gap appears as a polaritonic feature caused by resonance of each constitutive element rather than their spatial arrangement determining Bragg resonances [31]. In periodic structures, photonic crystal and metamaterial regime

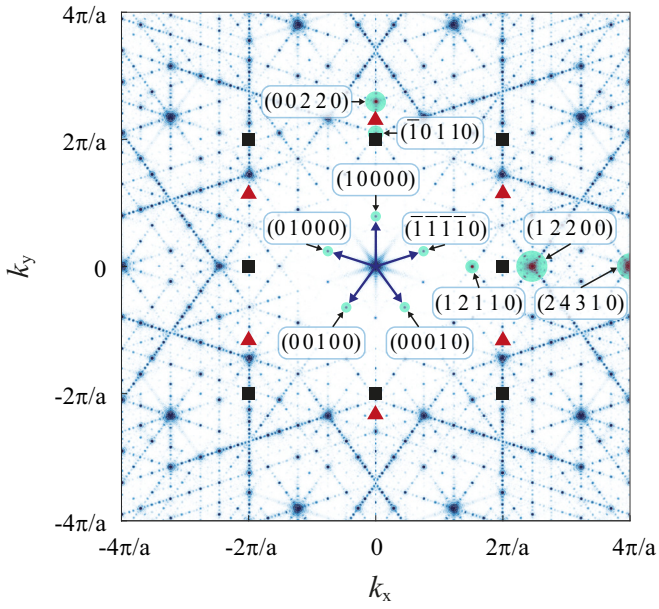

FIG. 3. Structural factor for hexagonal lattice (red triangles), square lattice (black square), and Penrose lattice (blue point). Blue arrows illustrate the representation of basis vectors described by five Miller indices for Penrose lattice. The maxima of the basis vectors and the maxima along two orthogonal directions (x and y axes) are highlighted with green points.

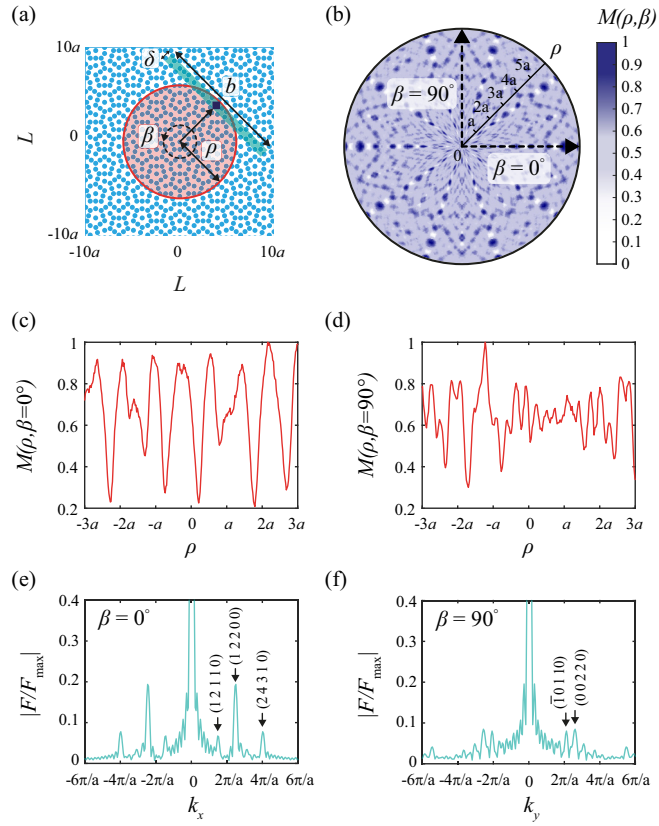

FIG. 4. (a) Illustration of the real-space metric procedure applicable for quasicrystals. (b) The result of the transformation is depicted in map $M(\rho, \beta)$. Sections of the map along radius ρ for angles (c) $\beta = 0^\circ$ and (d) $\beta = 90^\circ$. The Fourier transform of the sections along (e) $\beta = 0^\circ$ and (f) $\beta = 90^\circ$.

definitions are based on the behavior of the second dispersion branch in the band diagram, which determines the type of the lowest band gap. In the photonic crystal regime, the second branch has a minimum frequency at the boundary of the Brillouin zone and, in the metamaterial regime, the second branch has a minimum frequency at the center of the Brillouin zone (the Γ point) forming the polaritonlike feature. For some additional details see [44]. Unfortunately, this approach is not useful for quasicrystal structures because the band structure is poorly defined for the aperiodic systems. However, the structure factor of a quasicrystal lattice has a pattern comprising localized maxima similar to the case of periodic crystals, so that the structure factor is usually considered for the analysis of Bragg-type scattering in quasicrystals.

We constructed the structure factor of the extended Penrose lattice with $s = 0$ and compared it with the structure factor of hexagonal and square lattices (Fig. 3). The distance to the closest node in the reciprocal space defines the minimum of the Bragg resonances; thus the Mie resonance shift below this frequency allows the metamaterial regime to exist. As seen from Fig. 3 the distance between the nearest diffraction maximum and the Γ point ($\mathbf{k} = 0$) in the quasicrystal is much less than in a square or hexagonal lattice and, moreover, a condensation of maxima is observed. It is also worth noting that, in contrast to a periodic structure, a quasicrystal structure has a diffuse background, which is clearly visible in Fig. 3. Thus no minimal Bragg frequency exists for a structure with the quasicrystal lattice. This challenges the existence of a metamaterial regime in a quasicrystal structure.

Further research requires the introduction of basis vectors in reciprocal space. The reciprocal space for the quasicrystal can be constructed using five basis vectors [45]. We identify each node or maximum in the reciprocal space using five Miller indices ($hklmn$) vectors (see Fig. 3). The maxima along two orthogonal directions, i.e., the x and y axes, were defined by a sum of the basis vectors.

IV. REAL-SPACE METRIC

As mentioned above, a quasicrystal is an aperiodic structure, so it is impossible to identify the period in the same way as for the case of a photonic crystal. On the other hand, the Penrose lattice in reciprocal space (Fig. 3) contains a lot of maxima and each of them corresponds to a unique crystallographic plane. This complex diffraction pattern leads to the difficulty of visual identification of the crystallographic planes on which Bragg scattering takes place. For this reason, we need an appropriate numerical procedure. Previously, a real space self-convolution method was applied to quasicrystalline structures [19] to measure the periodicity degree. However, it could not help identify the planes. Here we developed another real-space method for the purpose.

Figure 4(a) illustrates the procedure applied to the structure. For a point in the real space with polar coordinates radius ρ and angle β, a narrow rectangular stripe orthogonal to the radius is considered [shown in cyan in Fig. 4(a)]. Next, we integrate a rod distribution binary function (one for points

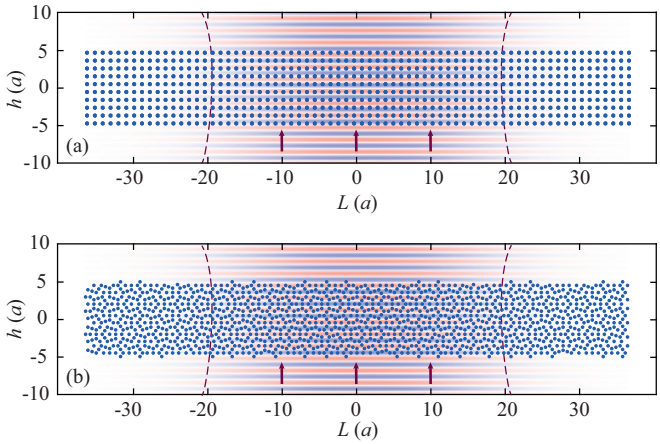

FIG. 5. Schematic representation of samples of $76a \times 10a$ size consisting of dielectric rods: (a) periodic structure; (b) quasicrystal structure. Red arrows show direction of incidence Gaussian beam. The background shows a Gaussian beam in free space. The red dotted lines show the width of the Gaussian beam.

occupied with rods and zero otherwise) over the area. We apply this procedure to the final size of Penrose tiling, so we also limit the size of the strip. We used the following dimensions for the stripe: the width $\delta = 2a$ and the length $b = 14.4a$. The strip sizes dimension choice is an accuracy-complexity trade-off. We used the sizes optimized to clearly identify crystallographic planes and reduce computation time. This procedure was applied to each point within a circle of radius $\rho = 6a$. As a result of such a transformation the map $M(\rho, \beta)$ shown in Fig. 4(b) was obtained. Each maximum in the map unveils a crystallographic plane oriented along the stripe.

Two sections of the map along $\beta = 0^\circ$ and $\beta = 90^\circ$ are shown in Figs. 4(c) and 4(d). The plots demonstrate alternations of minima and maxima which are superpositions of crystallographic planes. We apply Fourier transform to these data sets [Figs. 4(e) and 4(f), respectively]. The section along $\beta = 0$ is composed of three sets of planes; the period corresponds to maxima in the reciprocal space with Miller indices (12110), (12200), and (24310) labeled in Fig. 3. The orthogonal direction ($\beta = 90^\circ$) reveals two planes ($\bar{1}0110$) and (00220). We can notice that there are no traces of the first-order planes (00110), which resemble the case for crystals. It should be recalled that in particular a face-centered cubic lattice has no planes with Miller indices of different parity.

Thus, despite the aperiodicity of the quasicrystal, we have an implement to determine the period of the effective crystallographic planes.

V. TRANSMISSION SPECTRA

Transmission spectrum analysis is another useful tool that can be applied to finite structures. We consider rectangular periodic structures (PS) and quasicrystal structures (QS) with a length of $L = 76a$ along the x axis and different thickness h along the y axis. Figure 5 shows schematically the sample and incident Gaussian beam (red arrows in the figure) with a waist of $w = 20a$. As a source of incident field, we choose

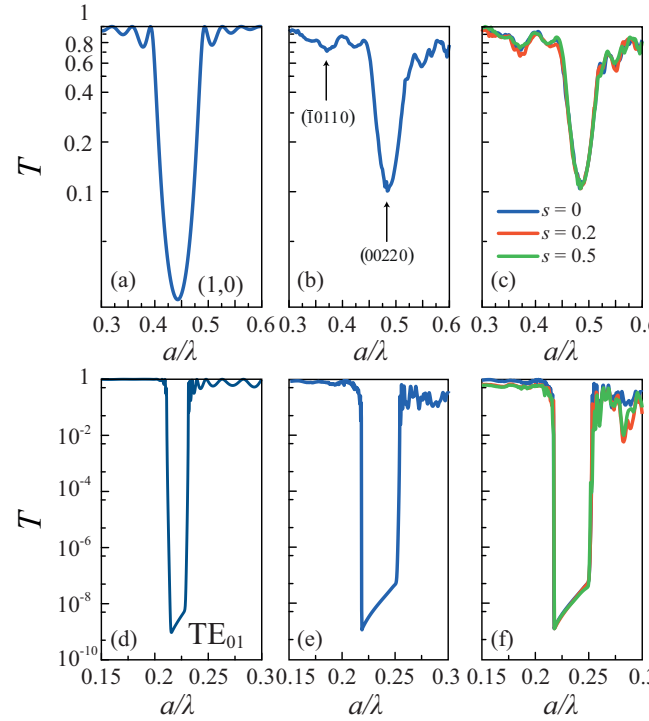

FIG. 6. Transmission spectra of photonic crystal with square lattice (a) and photonic quasicrystal with Penrose-type lattice (b). (c) Comparison of transmission spectra of quasicrystal structures with shift parameter $s = 0$ (green line), $s = 0.2$ (blue line), and $s = 0.5$ (red line). Transmission spectrum of metamaterial: (d) with square lattice; (e) with Penrose-type lattice. (f) Comparison of transmission spectra of metamaterials with shift parameter $s = 0$ (green line), $s = 0.2$ (blue line), and $s = 0.5$ (red line).

100 point dipole sources located along the horizontal line at a distance of $15a$. The transmitted signal is registered at the opposite size of the sample at the distance of $3a$ and averaged along the horizontal line of length $14a$, which is less than the waist. We use the multiple scattering theory to calculate transmission spectra and the electromagnetic field distribution inside the structure [46–49]. This method allows one to take into account not only the incident field of the source, but also the scattered field from neighboring rods.

It is instructive to compare low- and high-dielectric index cases for periodic and quasicrystalline structures having the same thickness $h = 10a$ and filling fraction $r/a = 0.25$. Figure 6(a) shows the transmission spectrum of a low-index photonic crystal with $\varepsilon = 4$. The spectrum exhibits a symmetrical dip at $a/\lambda = 0.44$, the shape of which is in compliance with the oval type complex dispersion at the Bragg band gap region [50]. The Bragg scattering occurs due to the interaction of the light cones with the origins at $\mathbf{k} = 0$ and $(1, 0) \times 2\pi/a$. We know from the diffraction theory that a wave with the wave vector $k = 2\pi n_{av}/\lambda$ diffracts with the event associated to maxima in the reciprocal space at the boundaries of the Brillouin zone $-\pi/a \leqslant k \leqslant \pi/a$. We define the average refractive index of the medium as $n_{av} = p_1 n_1 + p_2 n_2$, where p_1 and p_2 are positive weights for the refractive index n_1 and n_2, respectively. Thus, by using the proposed metric, we relate maxima in reciprocal space to the photonic band gaps.

For the considered structure and the (10) crystallographic plane, spacing $d = a$ and $\theta = 0$ and $n_{av} = 1.37$. Transmission spectrum of the quasicrystal is displayed in Fig. 6(b) with symmetric dip at $a/\lambda = 0.47$. The dip profile appears similar to those shown in Fig. 6(a) for the periodic structure. The Bragg law allows one to evaluate the crystallographic plane period $a_{\text{eff}} = 0.78a$, which corresponds to the (00220) planes revealed with the real-space metric. Moreover, we recognize the weak dip at $a/\lambda = 0.38$ as Bragg scattering on the $(\bar{1}0110)$ crystallographic plane. We examined transmission spectrum dependence on the shift parameter s and found it is almost negligible [see Fig. 6(c)].

Now we turn to the high-index structures with the same geometrical parameters but with rod permittivity $\varepsilon = 50$. The typical knife-shaped dip appears in the transmission spectra of periodic structure [Fig. 6(d)] and quasicrystal [Fig. 6(e)], which does not depend on the quasicrystal shift parameter [Fig. 6(f)] as it was observed for the low-index case. This feature has the same frequency as the magnetic dipole Mie resonance TE_{01}. For the periodic structures, the high frequency boundary is attributed to a μ-near zero metamaterial regime. We observe the same feature in the spectra of both periodic and aperiodic systems and the dip frequency does not depend on the lattice arrangement since it is the way in which the Mie resonance in each rod manifests itself spectrally.

The transmission spectrum of a periodic slab is known to comprise Fabry-Pérot fringes because of the wave reflection from the boundaries and the features arisen by the scattering event in the volume, which are Bragg or Mie scattering. Since volume-driven effects are described by Bloch solutions having the form of $\exp(i\mathbf{k}\cdot\mathbf{r})U(\mathbf{r})$, the logarithm of transmission around the dip is almost linear to the product of the imaginary part of the wave vector $\mathbf{k}$ and the thickness of the slab h. We simulated the transmission spectrum dip minimum as a function of the thickness for the Bragg dips for the low-index $\varepsilon = 4$ case [Fig. 7(a)] and the Mie dip at the knife-shaped tip for the high-index $\varepsilon = 50$ case [Fig. 7(b)]. The low-index structures demonstrate linear dependence for both periodic and quasicrystal lattices and the (10) Bragg dip of the photonic crystals decreases stronger with the slab thickness because of the perfect translation symmetry. The examined high-index structures show a strong drop of the transmission with saturation at a few first layers of dielectric rods. This property of the metamaterials is widely exploited in flat metasurfaces containing a single layer of resonant particles. The periodic structure has a stronger effect than for the low-index case. However, for the thicknesses of about $h = 10a$ and longer, the knife-shaped dip decrease is saturated due to the finite size of the simulated structure in the transverse dimension. It should be recalled that simulation of aperiodic structure does not allow Bloch boundary conditions along this direction, limiting the structure domain by the available computational memory.

The shift parameter determines the emergence of large scale domains that support the local modes observed in domain structures. As for structure with shift parameter $s = 0$, there are two orthogonal directions of alternation of maxima and minima in the maps for structures $s = 0.2$ and $s = 0.5$. There is almost no difference between the transformation maps, so the positions of crystallographic planes should be preserved with the change of the shift parameter. The Fourier

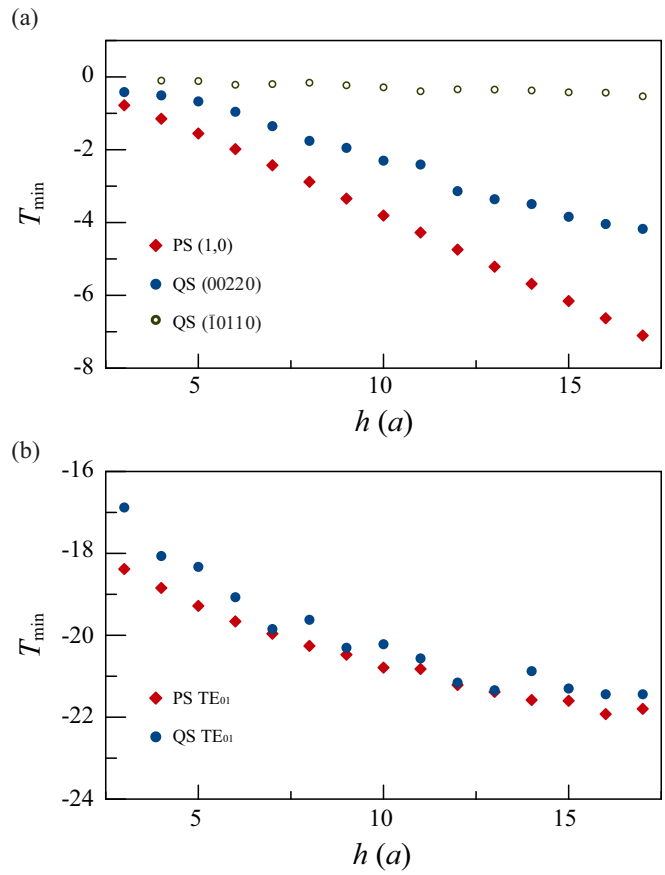

FIG. 7. Dependency of transmission spectra minimum on the width of structure. Solid red diamonds correspond to the square lattice, solid blue circles correspond to the main minimum of the (00220), and hollow green circles correspond to the second minimum in the photonic quasicrystal assigned to the $(\bar{1}0110)$.

transform reveals that the positions of the three sets of planes are preserved for all shift parameters. Consequently, for each crystallographic plane the effective period remains constant, so the transmission spectra almost do not change.

Overall, the analysis of transmission spectra reveals that the volume scattering processes in structures with the quasicrystal lattice are very similar to those observed in periodic photonic crystals. Moreover, the transmission dips related to the Mie modes supported by each element dominate the Bragg ones, the nature of which is in the spatial arrangement of the rods. Thus this analysis justifies the appearance of the metamaterial regime in structures with a quasicrystal lattice in spite of the condensation of maxima in the reciprocal space discussed above (Fig. 3).

VI. METAMATERIAL REGIME

The structure becomes a metamaterial when the conventional optical description of unusual effects is applicable, i.e., the propagation of electromagnetic waves can be described with extreme material parameters. Near-zero regimes for effective dielectric permittivity or magnetic permeability are well-recognized attributes of the metamaterial regime to appear [31,43]. In the periodic systems, the near-zero

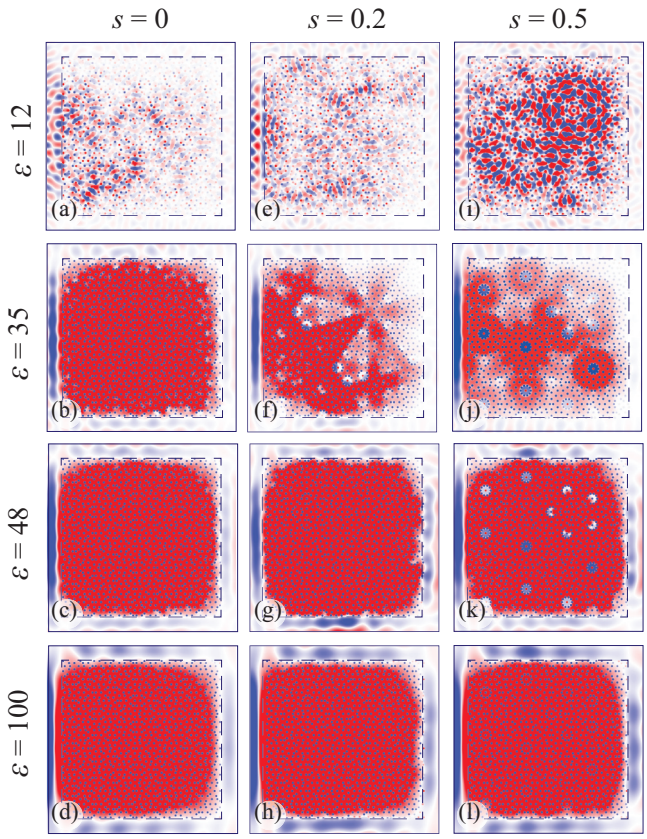

FIG. 8. Distributions of the magnetic field for the μ-near-zero modes in metamaterials with magnetic response. (a)–(d) $s = 0$, (e)–(h) $s = 0.2$, and (i)–(l) $s = 0.5$. Dark blue dashed lines show structure boundaries. $r/a = 0.4$, TE polarization.

regimes are related to the valley around the minimum at the Γ point since short wave vectors correspond to long wavelengths implying the subwavelength approximation regarding the structure element size. For the case of an aperiodic quasicrystal, the photonic band structure is ill defined; however, the homogeneous mode excitation in the structure uncovers that the structure acquires the metamaterial regime. We studied the field distributions of the electromagnetic field excited by an incident Gaussian beam in quasicrystal structures of square shape for the TE polarization. Three configurations of the Penrose tiling were considered: $s = 0$, $s = 0.2$, and $s = 0.5$ (Fig. 8). In the quasicrystals with small dielectric permittivity of the rods ($\varepsilon = 12$, which corresponds to semiconductors in optical range [51,52]), the field has a chaotic distribution independent of the shift parameter. However, for the rod permittivity exceeding a certain value, the homogeneous distribution of the field reveals the near-zero regime in the quasicrystal system. Figure 8 shows that for high enough permittivity the homogeneous mode is supported by the structures regardless of the shift parameter value; however, there are intermediate states with a structure of domains with the opposite phase of the field. A realization of such an extreme material of photonic structure can be made using ceramics or even distilled water. The latter exhibits a dielectric constant change from 50 to 81 in the microwave range [53].

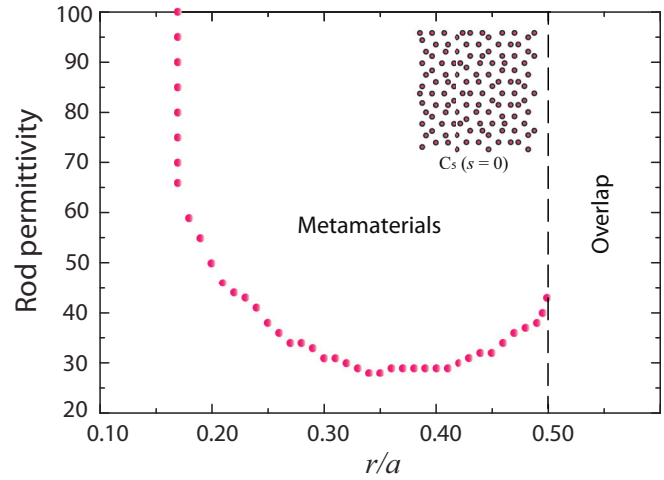

FIG. 9. Phase diagram of quasicrystal structure. Pink points show the area of metamaterial regime to appear. Inset shows the structure considered.

There are different ways to calculate the effective material parameters [32,54–57]. Here we consider a qualitative indicator, i.e., a homogeneous field distribution, when the electromagnetic field amplitude takes one sign in the whole volume of the structure. It is also worth noting that the near-zero magnetic permittivity μ_{eff} regime obtained in the present study agrees well with the calculations performed in accordance with Ref. [54]. Analyzing the appearance of a homogeneous field distribution in a quasicrystal structure, we constructed a phase diagram of metamaterial with the lattice based on Penrose tiling with a shift parameter $s = 0$ (see Fig. 9). The minimum value of the dielectric index of the constitutive element appears to be 28. The minimum of the rod permittivity ε in the quasicrystal structure with Penrose lattice is higher than for its periodic counterparts, yet the effect is clearly observed.

VII. CONCLUSIONS

We have shown the transport properties of electromagnetic waves when propagating through quasicrystal structures made of dielectric rods arranged in the nodes of a lattice based on a Penrose tiling with C_5 rotation symmetry. We have used the photonic crystal as a reference, which shows that quasicrystal structures have similar transmission suppression dependences on the thickness in the band gap of both types. A μ_{eff}-near-zero regime indicates that the structure acquires a metamaterial regime. We have constructed a phase diagram in the axes ($\varepsilon - r/a$), which determines the region of the metamaterial existence. Also, we have observed an intermediate state with domains in the structure with shift parameters $s = 0.2$ and $s = 0.5$.

ACKNOWLEDGMENT

We acknowledge support from the Russian Science Foundation (Grant No. 20-79-10316).

[1] S. E. Skipetrov, Phys. Rev. B **102**, 134206 (2020).
[2] M. Sbroscia, K. Viebahn, E. Carter, J.-C. Yu, A. Gaunt, and U. Schneider, Phys. Rev. Lett. **125**, 200604 (2020).
[3] Z. Wu and Y. Zheng, Adv. Opt. Mater. **6**, 1701057 (2018).
[4] Q. Fu, P. Wang, C. Huang, Y. V. Kartashov, L. Torner, V. V. Konotop, and F. Ye, Nat. Photon. **14**, 663 (2020).
[5] L. Du, M. R. Molas, Z. Huang, G. Zhang, F. Wang, and Z. Sun, Science **379**, 447 (2023).
[6] D. Wan, T. Li, S. Chen, W. Chen, H. Hu, S. Y. Set, S. Yamashita, L. Shen, Y. Zou, T. Liu *et al.*, Laser Photon. Rev. **17**, 2300398 (2023).
[7] L. Siedentop, G. Lui, G. Maret, P. M. Chaikin, P. J. Steinhardt, S. Torquato, P. Keim, and M. Florescu, arXiv:2403.08404.
[8] G. Shang, M. Eich, and A. Petrov, APL Photon. **5**, 060901 (2020).
[9] Z. Li, T. Ma, S. Li, W. Gu, L. Lu, H. Yang, Y. Dai, and R. Wang, ACS Nano **16**, 11473 (2022).
[10] A. Lonergan and C. O'Dwyer, Adv. Mater. Technol. **8**, 2201410 (2023).
[11] Z. Li, S. Li, and T. Ma, Adv. Opt. Mater. **11**, 2202370 (2023).
[12] N. Lassaline, R. Brechbühler, S. J. W. Vonk, K. Ridderbeek, M. Spieser, S. Bisig, B. le Feber, F. T. Rabouw, and D. J. Norris, Nature (London) **582**, 506 (2020).
[13] Y. Lim, B. Kang, S. J. Hong, H. Son, E. Im, J. Bang, and S. Lee, Adv. Funct. Mater. **31**, 2104105 (2021).
[14] N. Lassaline, D. Chelladurai, M. Kohli, R. Ulrich, Y. Glauser, D. Petter, J. Leuthold, and D. J. Norris, Fourier surface grating couplers for integrated photonics, *Integrated Photonics Research, Silicon and Nanophotonics* (Optica Publishing Group, Washington, DC, 2022).
[15] A. D. Sinelnik, I. I. Shishkin, X. Yu, K. B. Samusev, P. A. Belov, M. F. Limonov, P. Ginzburg, and M. V. Rybin, Adv. Opt. Mater. **8**, 2001170 (2020).
[16] O. Zilberberg, Opt. Mater. Express **11**, 1143 (2021).
[17] E. A. Koreshin and M. V. Rybin, Phys. Rev. B **105**, 024307 (2022).
[18] Y. Zhang, Z. Lan, Z. Lan, L. Hu, Y. Shu, X. Yuan, P. Guo, X. Peng, W. Chen, J. Li *et al.*, Opt. Lett. **48**, 2229 (2023).
[19] V. A. Chistyakov, M. S. Sidorenko, A. D. Sayanskiy, and M. V. Rybin, Phys. Rev. B **107**, 014205 (2023).
[20] M. Kohmoto, B. Sutherland, and K. Iguchi, Phys. Rev. Lett. **58**, 2436 (1987).
[21] A. Sinelnik, K. Samusev, M. Rybin, and M. Limonov, SN Appl. Sci. **1**, 1213 (2019).
[22] W. Jin, M. Song, X. Yue, and Y. Gao, Opt. Mater. **100**, 109719 (2020).
[23] M. Song, W. Jin, S. Fu, and Y. Gao, Results Phys. **52**, 106884 (2023).
[24] P. Wang, Q. Fu, V. V. Konotop, Y. V. Kartashov, and F. Ye, Nat. Photon. **18**, 224 (2024).
[25] J.-W. Dong, M.-L. Chang, X.-Q. Huang, Z. H. Hang, Z.-C. Zhong, W.-J. Chen, Z.-Y. Huang, and C. T. Chan, Phys. Rev. Lett. **114**, 163901 (2015).
[26] P. R. T., E. Di Gennaro, G. Abbate, and A. Andreone, Phys. Rev. B **84**, 125111 (2011).
[27] L. Maiwald, T. Sommer, M. S. Sidorenko, R. R. Yafyasov, M. E. Mustafa, M. Schulz, M. V. Rybin, M. Eich, and A. Y. Petrov, Adv. Opt. Mater. **10**, 2100785 (2022).
[28] S.-Y. Jeon, H. Kwon, and K. Hur, Nat. Phys. **13**, 363 (2017).
[29] Á. Andueza, K. Wang, J. Pérez-Conde, and J. Sevilla, J. Appl. Phys. **120**, 083101 (2016).
[30] V. Chistyakov, M. Sidorenko, A. Sayanskiy, and M. Rybin, JETP Lett. **117**, 742 (2023).
[31] E. E. Maslova, M. F. Limonov, and M. V. Rybin, Opt. Lett. **43**, 5516 (2018).
[32] I. Liberal and N. Engheta, Nat. Photon. **11**, 149 (2017).
[33] Y. Shi and M. L. Falk, Phys. Rev. B **73**, 214201 (2006).
[34] P. M. Piechulla, L. Muehlenbein, R. B. Wehrspohn, S. Nanz, A. Abass, C. Rockstuhl, and A. Sprafke, Adv. Opt. Mater. **6**, 1701272 (2018).
[35] S. Yu, C.-W. Qiu, Y. Chong, S. Torquato, and N. Park, Nat. Rev. Mater. **6**, 226 (2021).
[36] M. E. Mustafa, M. Eich, and A. Y. Petrov, Opt. Mater. Express **14**, 1281 (2024).
[37] J. Nakakura, P. Ziherl, J. Matsuzawa, and T. Dotera, Nat. Commun. **10**, 4235 (2019).
[38] H. Ma, Z. He, H. Li, T. Zhang, S. Zhang, C. Dong, and W. Steurer, Nat. Commun. **11**, 6209 (2020).
[39] R. Penrose, Bull. Inst. Math. Appl. **10**, 266 (1974).
[40] C. Janot, *Quasicrystals* (Springer, Berlin, 1994).
[41] M. Chodyn, P. Kuczera, and J. Wolny, Acta Crystallogr. A **71**, 161 (2015).
[42] E. E. Maslova and M. V. Rybin, J. Phys.: Conf. Ser. **1400**, 066017 (2019).
[43] M. V. Rybin, D. S. Filonov, K. B. Samusev, P. A. Belov, Y. S. Kivshar, and M. F. Limonov, Nat. Commun. **6**, 10102 (2015).
[44] M. V. Rybin, M. F. Limonov, and Y. S. Kivshar, *Semiconductors and Semimetals* (Elsevier, Waltham, MA, 2019), Vol. 100, pp. 13–43.
[45] K. J. Franke, Quasicrystal surfaces: Morphology, phase transitions and epitaxy, Ph.D. thesis, Freie Universitat Berlin, 2004.
[46] P. Markoš, Opt. Commun. **361**, 65 (2016).
[47] P. Markoš and V. Kuzmiak, Phys. Rev. A **94**, 033845 (2016).
[48] G. Tayeb and S. Enoch, J. Opt. Soc. Am. A **21**, 1417 (2004).
[49] A. A. Dmitriev and M. V. Rybin, Phys. Rev. A **99**, 063837 (2019).
[50] M. V. Rybin and M. F. Limonov, Phys. Rev. B **93**, 165132 (2016).
[51] A. E. Krasnok, D. S. Filonov, C. R. Simovski, Y. S. Kivshar, and P. A. Belov, Appl. Phys. Lett. **104**, 133502 (2014).
[52] R. Gaponenko, M. S. Sidorenko, D. Zhirihin, I. L. Rasskazov, A. Moroz, K. Ladutenko, P. Belov, and A. Shcherbakov, J. Appl. Phys. **134**, 014901 (2023).
[53] D. A. Chermoshentsev, E. V. Anikin, I. M. Fradkin, M. S. Sidorenko, A. A. Dudnikova, A. S. Kalganov, M. F. Limonov, N. A. Gippius, and S. A. Dyakov, Nanophotonics (2024), doi: 10.1515/nanoph-2024-0161.
[54] S. O'Brien and J. B. Pendry, J. Phys.: Condens. Matter **14**, 4035 (2002).
[55] I. Liberal, A. M. Mahmoud, Y. Li, B. Edwards, and N. Engheta, Science **355**, 1058 (2017).
[56] N. Kinsey, C. DeVault, A. Boltasseva, and V. M. Shalaev, Nat. Rev. Mater. **4**, 742 (2019).
[57] A. M. Mahmoud and N. Engheta, Nat. Commun. **5**, 5638 (2014).